7

Plasmonics of media with negative material parameters

An important and unique feature of materials with negative material parameters is their ability to support a variety of surface electromagnetic modes. These surface modes have electromagnetic fields that have maximum amplitude at the surface of the medium with negative material parameters and the fields decay exponentially inside both the bulk of the medium and in vacuum (or the positive medium) outside. This feature is well known and extensively studied in the case of metals or plasmas, which have negative dielectric coefficients, and the surface modes are called surface plasmon (Ritchie 1957, Raether 1986). On a metal surface, the surface plasmons are essentially collective excitations of electrons with the charges displaced parallel to the (real part of the) wave vector on the surface of the metal. The interior of the metal is, however, shielded from these electromagnetic fields and the wave amplitude decays into the bulk of the metal as in a regular conducting medium. These surface plasmon modes have also been termed Zenneck waves or Sommerfeld waves in the context of the ionosphere. Fig. 7.1 qualitatively represents a surface plasmon mode on the surface of a metal. These charge density waves flow on the surface, they scatter off obstacles on the plane, reflect and refract off interfaces between two surfaces: thus they can literally be considered two-dimensional entities that exist on the surface. Surface plasmons on a plane surface cannot directly interact with propagating radiation in vacuum and are coupled mainly through scattering events (surface roughness, Bragg scattering in the case of periodic scatterers such as a diffraction grating, etc.). There are also localized surface plasmons that can be confined to the surface of a sphere, a cylinder or, in general, any scatterer made of a negative dielectric medium. These plasmons can be directly excited by an incident plane wave of light.

The surface plasmons become approximately degenerate for larger wavevectors on a metal surface. This is the essential reason why modeling the interaction of radiation with metallic structures of complex shape is so difficult – the radiation couples (through scatterers) to the surface plasmons at all lengthscales near the resonant frequencies. The surface plasmons have a P-polarized nature (TM polarization) on a metal surface. Apart from sensor applications, the main attraction for studying the properties of propagation and confinement of plasmons on metallic surfaces is the promise that

© 2009 by Taylor & Francis Group, LLC

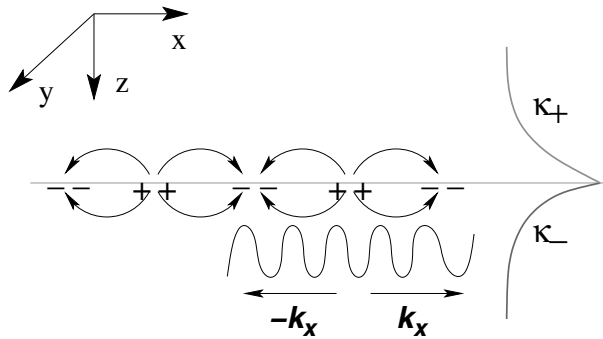

Figure 7.1 Schematic representation of a surface plasmon at an interface between a negative and a positive dielectric medium, and the associated charge density fluctuations. The exponential decay of the fields normal to the surface and the propagating nature along the surface are depicted schematically. (Reproduced with permission from (Ramakrishna 2005). © 2005, Institute of Physics Publishing, U.K.)

plasmons hold for miniaturization of all-optical circuits and communication devices. Photonic components due to photonic bandgap materials or conventional waveguides are just too bulky for integration with nonsecular electronic components. With surface plasmons, however, the wavelength on the surface can be much smaller than the wavelength of free radiation. This has implications for the possible miniaturization of the waveguides, the circuit channels, etc. required for optical switches and digital logic circuits. There can also be large local field enhancements due to the excitation of localized resonances, which implies that nonlinear effects can be made large, thus enabling easy switching of optical pulses. This has been the main driving force behind basic research on the control of surface plasmons on a metal surface. For more detailed discussions of surface plasmon modes on metallic surfaces, we refer the reader to Maier (2007).

The study of surface plasmons has regained interest and importance with the realization of metamaterials, in particular due to the possibility of reaching negative permeabilities. Until now, only P-polarized (TM-modes) surface plasmons could be excited on a metallic surface due to the necessity of having a normal component of the electric field. The possibility of having negative magnetic permeability gives rise to a electromagnetic modes of an alternate magnetic nature for the S-polarized waves (TE-modes) as well. This can give rise to new polarization-dependent phenomena in metamaterials shaped into complex geometrical shapes. In this chapter, we discuss, mainly in the context of metamaterials, some of the basic aspects of surface plasmon modes, their dispersion and interaction with radiation, and negative refraction at the interface between two surfaces. We also explore some sub-wavelength

© 2009 by Taylor & Francis Group, LLC

structured conducting films that show plasmonic responses. Surface modes on nonlinear metamaterials are briefly touched upon toward the end of the chapter.

7.1 Surface electromagnetic modes in negative refractive materials

In this section, we primarily focus on the conditions for the existence of surface plasmon modes and their dispersion in a variety of geometries and materials. The plasmon modes turn out to be crucial for the performance of a super-lens that can image the evanescent near-field modes of a source (see Chapter 8). An understanding of the conditions under which they exist and can be excited is important. The dispersive properties of the surface plasmons are discussed assuming a *local* response for the media concerned whereby the material parameters such as the dielectric permittivity (ε) and the magnetic permeability (μ) depend only on the frequency ω and are not spatially dispersive.

7.1.1 Surface plasmon modes on a plane interface

The dispersive properties of surface plasmon modes on the surface of a semi-infinitely extended negative refractive index medium have been considered in Ruppin (2000b). Let us consider the interface ($z = 0$ plane) between two semi-infinitely extended media whose material parameters are given by (ε_1, μ_1) and (ε_2, μ_2). Consider the time harmonic fields at frequency ω in the two media for P-polarized light (magnetic field along the y axis):

$$\mathbf{H}(x,y,z) = \begin{cases} \hat{y}H_2 \exp[\mathrm{i}(k_x x + k_y y - \omega t) - \kappa_{z2} z], \forall \quad z > 0, \\ \hat{y}H_1 \exp[\mathrm{i}(k_x x + k_y y - \omega t) + \kappa_{z1} z], \forall \quad z < 0, \end{cases} \tag{7.1}$$

where $k_x^2 + k_y^2 - \kappa_{z1}^2 = \varepsilon_1 \mu_1 \omega^2/c^2$ and $k_x^2 + k_y^2 - \kappa_{z2}^2 = \varepsilon_2 \mu_2 \omega^2/c^2$. Note that the fields decay exponentially away from the interface into the bulk of the media in either side. The transverse components of both fields are the same due to the translation invariance along the transverse directions (necessity of phase matching). The coefficients H_1 and H_2 in the above equations are solved for by enforcing the conditions of continuity of the tangential magnetic field and the electric field across the interface:

$$H_2 - H_1 = 0, \qquad \frac{\kappa_{z2}}{\omega \varepsilon_2} H_2 + \frac{\kappa_{z1}}{\omega \varepsilon_1} H_1 = 0. \tag{7.2}$$

This system of homogeneous equations has a non-trivial solution when the determinant is zero:

$$\frac{\kappa_{z1}}{\varepsilon_1} + \frac{\kappa_{z2}}{\varepsilon_2} = 0, \tag{7.3}$$

© 2009 by Taylor & Francis Group, LLC

which is the condition for the existence of the surface modes. It is obvious that solutions to this equation require that the permittivities of the two media be of opposite signs.

¿From the above condition, the dispersion for these surface modes is obtained as

$$k_x = \left[\frac{\varepsilon_1\varepsilon_2(\varepsilon_2\mu_1 - \varepsilon_1\mu_2)}{\varepsilon_2^2 - \varepsilon_1^2}\right]^{1/2}\frac{\omega}{c}. \tag{7.4}$$

A similar condition for S-polarized light (electric field along the $\hat{y}$ direction) can be obtained as

$$\frac{\kappa_{z1}}{\mu_1} + \frac{\kappa_{z2}}{\mu_2} = 0, \tag{7.5}$$

which obviously requires only one of the μ involved be negative. We can similarly obtain the dispersion for these surface modes as

$$k_x = \left[\frac{\mu_1\mu_2(\mu_2\varepsilon_1 - \mu_1\varepsilon_2)}{\mu_2^2 - \mu_1^2}\right]^{1/2}\frac{\omega}{c}. \tag{7.6}$$

Note that the P-polarized and S-polarized modes do not coexist at any frequency except where $\varepsilon_2\mu_2 = 1$.

In order to understand the dispersion of these surface modes, it is important to consider causal, frequency dispersive models for the negative permittivity and permeability. Let us, as usual, consider a plasma model for the dielectric permittivity (see Section 3.1),

$$\varepsilon_2 = 1 - \frac{\omega_p^2}{\omega(\omega + \mathrm{i}\gamma_p)}, \tag{7.7}$$

where the plasma frequency is ω_p and a magnetic resonance model for the magnetic permeability (see Section 3.2) is:

$$\mu_2 = 1 + \frac{f\omega^2}{\omega_{0m}^2 - \omega^2 - \mathrm{i}\omega\gamma_m}, \tag{7.8}$$

where the magnetic plasma frequency (when $\mu_2 = 0$) is given by $\omega_{mp}^2 = \omega_{0m}^2/(1-f)$. While investigating the dispersion of these modes, let us assume the limit of zero damping $\gamma_p \to 0$ and $\gamma_m \to 0$. Let us take the positive media to have $\varepsilon_1 = 1$, $\mu_1 = 1$.

The dispersion for the cases of the P-polarized and the S-polarized surface modes are shown in Fig. 7.2. Note that the surface modes exist only for frequencies when the waves are evanescent in both media. This requires $k_x^2 > \omega^2/c^2$ and $k_x^2 > \varepsilon_2\mu_2\omega^2/c^2$. It can be seen from the figure that the P- and S-polarized modes become degenerate for large wave-vectors k_x at the frequencies $\omega = \omega_{0m}$, $\omega_p/\sqrt{2}$ and $\omega = \omega_{ms} = \omega_{0m}/\sqrt{1 - f/2}$, respectively. For the parameters associated with the graph on the top panel of Fig. 7.2, there are two branches of the P-polarized modes: one at low frequencies for

© 2009 by Taylor & Francis Group, LLC

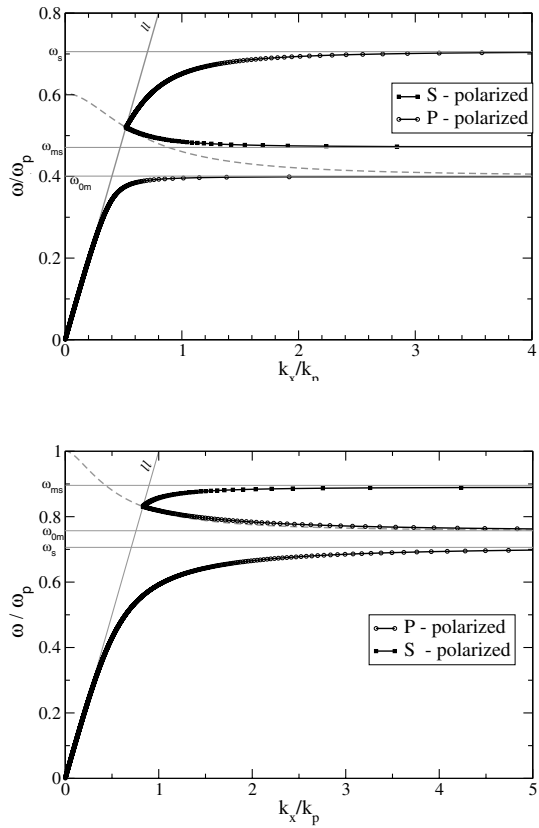

Figure 7.2 Top panel: Dispersion of the surface plasmon modes for a medium with the material parameters given by Eqs. (7.7) and (7.8). There are two branches for the P-polarized modes (with positive slope) and one for the S-polarized mode (negative slope). The assumed parameters are $\omega_{0m} = 0.4\omega_p$, $f = 0.56$. Bottom panel: Dispersion of the surface plasmon modes for a medium with $\omega_{0m} = 0.75\omega_p$, $f = 0.56$. Note that when $\omega_{mp} > \omega_p$ the dispersion curves for the S- and P-polarized modes change the sign of their slopes. In both panels, the light line ($\omega = ck_x$) indicated as "*ll*" and the curve $k_x = \varepsilon(\omega)\mu(\omega)\omega^2/c^2$ (dashed curve) are indicated in grey. The surface modes can occur only to the right of these curves. The dielectric surface plasmon frequency ω_s when $\varepsilon_2 = -1$, the magnetic surface mode frequency ω_{ms} when $\mu_2 = -1$, and the magnetic resonance frequency ω_{0m} are indicated by grey lines in both panels.

$\omega < \omega_{0m}$ where $\varepsilon_2 < 0$ while $\mu_2 > 0$ and is large near the resonance, and

© 2009 by Taylor & Francis Group, LLC

another one for $\omega < \omega_p$. The low frequency P-polarized branch is the only branch present for an interface between vacuum and a metal with $\varepsilon_2 < 0$. Part of the second branch lies in the spectral region where both $\mu_2 < 0$ and $\varepsilon_2 < 0$, thus in a region of negative refractive index. This branch essentially originates on the intersection of the light line in medium 1 ($k_x = \sqrt{\varepsilon_1\mu_1}\omega/c$) and the curve $k_x > \sqrt{\varepsilon_2\mu_2}\omega/c$. There is, by comparison, only one branch for the S-polarized mode that lies entirely within the left-handed regime where $\varepsilon_2 < 0$ and $\mu_2 < 0$. Note that the locations of the high frequency branch for the P-polarized mode and the S-polarized mode are interchanged if we choose $\omega_{mp} > \omega_p$. This is shown in the bottom panel of Fig. 7.2 where $\omega_{0m} = 0.75\omega_p$ and $f = 0.56$. It can be seen that when the magnetic plasma frequency $\omega_{mp} > \omega_p$ the S-polarized mode has a positive slope while the P-polarized mode has negative slope. In this case, we also have that both the high frequency S and P modes lie entirely within the region of negative refractive index, i.e., when $\varepsilon_2 < 0$ and $\mu_2 < 0$. Note that our treatment includes the surface modes at the interface between the two media if $\varepsilon_1 < 0,\ \mu_1 > 0$ and $\varepsilon_2 > 0,\ \mu_2 < 0$, in which case, there are no propagating modes in either of the two media as $k_x^2 > \varepsilon_1\mu_1\omega^2/c^2$ and $k_x^2 > \varepsilon_2\mu_2\omega^2/c^2$ for all k_x, however small.

In the previous discussion, the dissipation in the medium was neglected while examining the dispersion of the surface plasmon modes. When a finite imaginary part is introduced into the negative medium parameters, the transverse wave-vector becomes complex. The imaginary part corresponds to the inverse propagation length on the surface. The surface plasmon amplitude decays to $1/e$ of its initial values while propagating over this length. Due to the algebraic complexity of the expressions, it is fruitful to examine them separately for different cases.

(*i*) *A negative dielectric metal*: For case of a metal with only $\varepsilon_2 < 0$ and $\mu_2 = \mu_1 = 1$, we can simplify the dispersion equation for the P-polarized modes to

$$k_x = \left(\frac{\varepsilon_1\varepsilon_2}{\varepsilon_1 + \epsilon_2}\right)^{1/2} \frac{\omega}{c}, \tag{7.9}$$

Noting that $\varepsilon_1 = \varepsilon_2' + \mathrm{i}\varepsilon_2''$, in the limit $\varepsilon_2'' \ll \varepsilon_2'$ we obtain

$$k_x \approx \left(\frac{\varepsilon_2'}{\varepsilon_1 + \varepsilon_2'}\right)^{1/2} \frac{\omega}{c} + \mathrm{i}\left(\frac{\varepsilon_2'}{\varepsilon_1 + \varepsilon_2'}\right)^{3/2} \frac{\varepsilon_2''}{2(\varepsilon_2')^2} \frac{\omega}{c}. \tag{7.10}$$

In order to satisfy the conditions for a surface plasmon mode, we require $\varepsilon_2 < 0$, and for real k_x' an additional requirement is $|\varepsilon_2'| > \varepsilon_1$. The propagation length for the surface plasmon is

$$\ell_{sp} = \{2\mathrm{Im}(k_x)\}^{-1}. \tag{7.11}$$

For surface plasmons on silver at about 500 nm wavelength radiation, the propagation length evaluates to about $\ell_{sp} \simeq 20\ \mu$m. Basically as $|\varepsilon_2'|$ increases, the fields penetrate lesser into the metal and the consequent losses are lesser.

© 2009 by Taylor & Francis Group, LLC

At about 1200 nm wavelength, the surface plasmon propagation length in comparison comes out to be about 1 mm. To measure ℓ_{sp}, we would need to inject energy in the surface modes at one point and measure the fields of the mode some distance away, which can be accomplished by near-field microscopy techniques (Paesler and Moyer 1996). Another related quantity that is of interest is the decay time of the surface plasmon which can be probed by a pulse of light. Upon considering k_x to be a real quantity (excitation by a plane wave), the real and imaginary parts of the complex frequency are given by

$$\omega' - \mathrm{i}\omega'' = (k_x c)\left(\frac{\varepsilon_1 + \varepsilon_2'}{\varepsilon_1 \varepsilon_2'}\right)^{1/2} - \mathrm{i}(k_x c)\frac{\varepsilon_2''}{2{\varepsilon_2'}^2}\left(\frac{\varepsilon_1 \varepsilon_2'}{\varepsilon_1 + \varepsilon_2'}\right)^{1/2}. \tag{7.12}$$

The imaginary part of the frequency is negative and represents the rate of dissipation in the medium, whereas the decay time is inversely proportional to this and $t_{sp} = (2\pi)/\omega''$. The spatial decay length on the surface and the decay time are related by $\ell_{sp} = v_g t_{sp}$, where v_g is the group velocity on the surface.

(*ii*) *Interface between vacuum and a negative refractive index medium*: Let us consider the case when $\varepsilon_1 = 1$ and $\mu_1 = 1$. Then the dispersion reduces to

$$k_x = \left[\frac{\varepsilon_2(\varepsilon_2 - \varepsilon_1)}{\varepsilon_2^2 - 1}\right]^{1/2}\frac{\omega}{c}. \tag{7.13}$$

We can separate the real and imaginary parts of the right-hand side in the limit of $\varepsilon_2'' \ll \varepsilon_2'$ and $\mu_2'' \ll \mu_2'$ in a straightforward but slightly tedious calculation and obtain

$$k_x' \approx \left[\frac{\varepsilon_2'(\varepsilon_2' - \mu_2')}{{\varepsilon_2'}^2 - 1}\right]^{1/2}\frac{\omega}{c}, \tag{7.14}$$

$$k_x'' \approx \left[\varepsilon_2''\frac{(\varepsilon_2'\mu_2' + 2)({\varepsilon_2'}^2 - \mu_2'\varepsilon_2')^{1/2}}{({\varepsilon_2'}^2 - 1)^{3/2}} - \mu_2''\left(\frac{\varepsilon_2'}{({\varepsilon_2'}^2 - 1)(\varepsilon_2' - \mu_2')}\right)^{1/2}\right]\frac{\omega}{2c}. \tag{7.15}$$

It is clear that the additional possibility of having a negative magnetic permeability increases the number of possibilities. Given that $\varepsilon_2 < 0$, we require for real k_x' that

$$\frac{(\varepsilon_2' - \mu_2')}{{\varepsilon_2'}^2 - 1} > 0.$$

This implies that the imaginary part of the magnetic permeability can actually increase the propagation length via a phase shift in the fields compared to the case when $\mu_2'' = 0$. Surprising as this result might seem, one should

© 2009 by Taylor & Francis Group, LLC

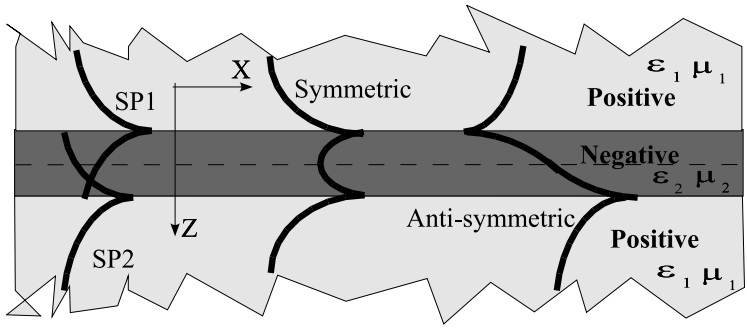

Figure 7.3 Schematic representation of the geometry of the slab of a material with negative ε or μ. The surface plasmons on two interfaces are no longer independent and get coupled to give rise to coupled slab plasmon polariton excitations. The slab modes can have field distributions that are either symmetric or anti-symmetric with respect to the center of the slab.

remember that the total dissipation is due to both the electric and magnetic susceptibilities. We discuss the full implications for the real part of k_x', and the possibility of negative refraction for the surface plasmon in Section 7.3.

The most important aspect about all these modes is that all of them lie to the right of the dispersion of free light (shown by the dotted curve in the figures). This implies that propagating modes of light incident on the surface can never couple to these surface plasmon modes as the phase matching condition can never be satisfied. The surface plasmon modes can, however, be excited through a periodic structure on the surface where the Bragg scattering for propagating modes can give the extra wave-vector (momentum) along the transverse direction. As another example, surface roughness can also accomplish the same effect (the surface roughness can be considered to be a "white" distribution of different frequencies). Alternatively, they can be excited by the near-field evanescent modes of a source placed very close by. These aspects have been very thoroughly discussed in Raether (1986) for the case of surface plasmon modes on a metal surface.

7.1.2 Surface plasmon polariton modes of a slab

The surface plasmon modes in a slab of a medium with negative material parameters and a finite thickness d are interesting since a slab has two interfaces where degenerate surface plasmon modes can be supported (see Fig. 7.3). Each interface plasmon feels the fields of the surface plasmon on the other interface, and they hybridize to form a pair of non-degenerate slab modes. The problem is completely analogous to the problem of quantum levels in two identical potential wells separated by some distance.

© 2009 by Taylor & Francis Group, LLC

Consider that the slab has a width d, material parameters (ε_2, μ_2) given by Eqs. (7.7) and (7.8), and is embedded in a medium whose material parameters are (ε_1, μ_1). The conditions for the existence of independent slab modes can be obtained in a similar manner by matching the tangential components of the electric and magnetic fields across the two interfaces. Note that the fields inside the slab can be written as a superposition of an exponentially decaying and an exponentially amplifying wave along the thickness of the slab. The conditions for the P-polarized modes come out to be

$$\tanh(\kappa_{z2}d/2) = -\frac{\varepsilon_2\kappa_{z1}}{\varepsilon_1\kappa_{z2}}, \tag{7.16a}$$

$$\coth(\kappa_{z2}d/2) = -\frac{\varepsilon_2\kappa_{z1}}{\varepsilon_1\kappa_{z2}}, \tag{7.16b}$$

where $\kappa_{zj} = \sqrt{k_x^2 - \varepsilon_j\mu_j\omega^2/c^2}$. Each of these conditions corresponds to a slab mode. The two modes have different symmetries of the fields with respect to the center of the slab: one has a symmetrical field distribution $(\cosh[\kappa_z(z - d/2)])$ while the other has an anti-symmetric field distribution $(\sinh[\kappa_z(z - d/2)])$ corresponding to the first and the second conditions of Eq. (7.16), respectively. Thus, the slab develops a gross polarization and hence these modes are called surface plasmon polariton (SPP) modes. Similarly the conditions for the S-polarized modes are

$$\tanh(\kappa_{z2}d/2) = -\frac{\mu_2\kappa_{z1}}{\mu_1\kappa_{z2}}, \tag{7.17a}$$

$$\coth(\kappa_{z2}d/2) = -\frac{\mu_2\kappa_{z1}}{\mu_1\kappa_{z2}}. \tag{7.17b}$$

The dispersions for the slab plasmon polaritons have to be obtained as the solution to the above transcendental equations. These dispersion relations are plotted in Fig. 7.4. In fact, if we calculate the transmission or reflection coefficients for light incident on the slab, the conditions for the SPP modes correspond to the poles of the transmission or reflection coefficient. This is a typical effect whenever a system is excited at resonance – the scattering coefficients (transmission and reflection coefficients in this case) diverge. We see that there are six branches in total: four for the P-polarized modes and two for the S-polarized modes. Basically each surface plasmon branch for the semi-infinite media splits into two separate branches. The separation of the branches that have hybridized reduces as the thickness of the slab increases and the branches merge asymptotically as $d \to \infty$. Once again the SPP can only exist in regions in the $(k_x,\ \omega)$ plane where $k_x^2 > \varepsilon_j\mu_j\omega^2/c^2$ in either of the two media. The lower two P-polarized branches for $\omega < \omega_{0m}$ occur in the region $\varepsilon_2 < 0,\ \mu_2 > 0$; the two S-polarized branches occur entirely within the negative refractive index band when $\varepsilon < 0,\ \mu_2 < 0$. The higher frequency P-polarized modes cross over to the region of $\varepsilon_2 < 0,\ \mu_2 > 0$ from the region of negative refractive index. For large wave-vectors, the slab polariton modes (for all k_x) become degenerate at ω_{0m} for the low frequency P-polarized modes,

© 2009 by Taylor & Francis Group, LLC

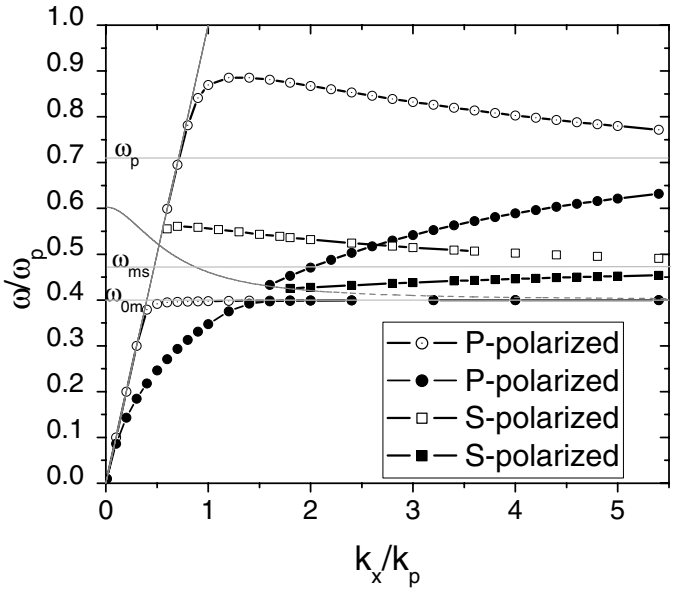

Figure 7.4 Dispersion of the slab plasmon polariton modes for a medium with the material parameters given by Eqs. (7.7) and (7.8). The surface plasmon branches essentially split into two modes: one symmetric and another anti-symmetric. The assumed parameters are $\omega_{0m} = 0.4\omega_p$, $f = 0.56$, and $k_p d = 0.3$. The light line ($\omega = ck_x$) and the curve $k_x = \varepsilon(\omega)\mu(\omega)\omega^2/c^2$ (dashed curve) are indicated in grey. The surface modes can occur only to the right of these curves. The dielectric surface plasmon frequency ω_s when $\varepsilon_2 = -1$, the magnetic surface mode frequency ω_{ms} when $\mu_2 = -1$, and the magnetic resonance frequency ω_{0m} are indicated by grey horizontal lines.

at $\omega = \omega_p/\sqrt{2}$ for the high frequency P-polarized modes, and $\omega = \omega_{ms}$ where the $\mu = -1$ for the S-polarized modes.

We also note that, for $\omega > \omega_{0m}$, the branches of the anti-symmetric P-polarized and S-polarized modes smoothly cross over to the dispersion of the first-order slab waveguide mode in the negative refractive index medium when the light is propagating inside the negative refractive index slab ($k_x^2 < \varepsilon_2\mu_2\omega_2/c^2$) and evanescent outside ($k_x^2 > \varepsilon_1\mu_1\omega^2/c^2$). We discuss waveguide modes separately in the next section.

In the quasi-static limit of $k_x \gg \omega/c$, we can easily obtain an analytic expression for the dispersion of the SPP modes. In this limit, $\kappa_{zi} \to k_x$ and the P-polarized modes becomes independent of μ while the S-polarized modes become independent of ε. Note that this does not hold for the P-polarized

© 2009 by Taylor & Francis Group, LLC

modes when $\mu_2 \to \infty$ as $\omega \to \omega_{0m}$. One can analytically obtain the dispersion for the P-polarized modes as

$$\omega_{\pm} = \frac{\omega_p}{2}[1 \pm \exp(-k_x d)]^{1/2}, \tag{7.18}$$

where the $\pm$ sign indicates the frequencies of the two non-degenerate modes. For the S-polarized modes, with the magnetic resonance model we obtain the dispersion as

$$\omega_{\pm} = \frac{\omega_{0m}}{1 - f/2[1 \pm \exp(-k_x d)]^{1/2}}. \tag{7.19}$$

Note that had we used a Lorentz model for the dispersion of μ_2, we would instead obtain

$$\omega_{\pm} = \left[\omega_{0m}^2 + \frac{\omega_b^2}{2}(1 \pm e^{-k_x d})\right]^{1/2}. \tag{7.20}$$

These equations illustrate the splitting of the modes and that the symmetric mode ω_+ has a higher frequency.

One should note that these results in the non-retarded regime should be treated as only approximate, particularly very close to the surface plasmon frequency. For example, the dispersions of both the symmetric and the anti-symmetric modes, at large slab thickness or large k_x, have to tend to the uncoupled plasmon dispersion for a single surface as the two plasmons are essentially uncoupled. Thus, even the slopes of the dispersion curves should be the same for large k_x. The non-retarded approximation predicts opposite signs for the group velocity on the surface, $(\partial\omega)/(\partial k_x)$. In reality, however, the two curves actually tend to the surface plasmon frequency either both from below (for $\omega_{mp} < \omega_p$) or both from above (for $\omega_{mp} > \omega_p$). In the former case, the upper dispersion curve crosses over to below ω_s at some point (Ramakrishna et al. 2002). This can have important physical implications: in the case of the silver lens discussed in Section 8.2.2, this would imply that the anti-symmetric mode is always excited.

Consider next the dissipation and the propagation of SPP modes in very thin slabs of the negative material. For concreteness, we consider the P-polarized modes only and the case of a metal ($\mu_2 = 1$, $\varepsilon_2 < 0$). In this case, several researchers (Kovacs and Scott 1977, Quail et al. 1981, Sarid 1981) reported both theoretic and experimental results that the damping for the symmetric mode reduces as the thickness of the metallic film decreases as much by an order of magnitude while the damping for the anti-symmetric mode increases by modest amounts. We can easily estimate the thickness dependence of the imaginary part of k_x for very thin films: using $\tanh(x) \sim x$ for $x \ll 1$ in Eq. (7.16), and for the symmetric mode $k_x = k_1 + \Delta$ where $k_1 = \varepsilon_1\omega^2/c^2$ and $\Delta \ll k_0$, we obtain that

$$\frac{\Delta}{\omega/c} \simeq \frac{\varepsilon_1(\varepsilon_1 - \varepsilon_2)^2(k_0 d/2)^2}{2[\varepsilon_2^2 - \varepsilon_1^2(\varepsilon_2 - \varepsilon_2)d^2k_0^2]}, \tag{7.21}$$

© 2009 by Taylor & Francis Group, LLC

from which we obtain in the limit of small $k_1 d$, the imaginary part of the wave-vector as

$$\frac{k_x''}{\omega/c} = \varepsilon_1(\varepsilon_2' - \varepsilon_1)\frac{\varepsilon_2''}{\varepsilon_2'^{\,2}}\left(\frac{k_1 d}{2}\right)^2, \tag{7.22}$$

which clearly demonstrates that $\ell_{sp} \sim d^{-2}$, i.e. the damping reduces with reducing thickness of the slab. This property is due to the field structure that is more spread out in the surrounding medium than inside the slab where dissipation takes place. It can be similarly shown that the damping actually increases but more moderately for the anti-symmetric SPP mode. More exact estimates can of course be obtained by solving Eq. (7.16) numerically for the real and imaginary parts of the wave-vector ($k_x = k_x' + ik_x''$) and such analyses indicate that a reduction in k_x'' by one order of magnitude is possible when the film thickness becomes of the order of 20 nm (Sarid 1981, Raether 1986). Such SPP modes would have an enhanced range of propagation on the surface and they are, therefore, referred to as *long range plasmons* (Sarid 1981). These long range plasmons penetrate highly into the surrounding media, and their potential for sensor applications at almost single molecule sensitivity and enhanced nonlinear phenomena has been demonstrated.

Finally, we consider the case when the slab has an asymmetric environment. This is typical of many applications, say, a silver film (ε_2) deposited on a quartz substrate (ε_1) with vacuum/air ($\varepsilon_0 = 1$) on the other side. The dispersion of the SPP modes can be determined by locating the poles of the transmission or the reflection coefficients (see Appendix C) in the (k_x, ω) plane. The condition for P-polarized light is

$$\left(\frac{\kappa_{z1}}{\varepsilon_1} + \frac{\kappa_{z2}}{\varepsilon_2}\right)\left(\frac{\kappa_{z1}}{\varepsilon_1} + \frac{\kappa_{z0}}{\varepsilon_0}\right) + \left(\frac{\kappa_{z1}}{\varepsilon_1} - \frac{\kappa_{z2}}{\varepsilon_2}\right)\left(\frac{\kappa_{z1}}{\varepsilon_1} - \frac{\kappa_{z0}}{\varepsilon_0}\right) e^{i\kappa_{z2} d} = 0. \tag{7.23}$$

For complex ε_1 and ε_2, one needs to determine the complex roots k_x of this equation. One tractable way to determine the roots is to scan the (k_x, ω) plane and monitor the derivative of the phase of the transmission coefficient. The phase changes rapidly in the vicinity of a resonance and the derivative shows a peak at the resonance. The main effects of the asymmetry are to give rise to a shift in the real part of k_x. In addition, when the wave can propagate in the substrate medium, it also gives a contribution to the imaginary part of k_x which corresponds to the energy radiated by the surface plasmon into the substrate medium. Fig. 7.4 showing the dispersion of the slab plasmon polariton modes, albeit for a symmetric slab, should be compared to Fig. 6.9 where similar information about the dispersion can be obtained from the frequency derivative of the phase of the transmission coefficient.

© 2009 by Taylor & Francis Group, LLC

7.2 Waveguides made of negative index materials

The guidance condition listed in Eqs. (7.16) and (7.17) can be studied in a more systematic manner in order to visualize the evolution of the associated modes with some typical parameters, such as the frequency and the thickness of the slab. In order to render the equations symmetric and with only dimensionless quantities, Eqs. (7.17) are rewritten as

$$\kappa_{z1}d = -\frac{\mu_1}{\mu_2}(\kappa_{z2}d)\tanh\left(\frac{\kappa_{z2}d}{2}\right), \tag{7.24a}$$

$$\kappa_{z1}d = -\frac{\mu_1}{\mu_2}(\kappa_{z2}d)\coth\left(\frac{\kappa_{z2}d}{2}\right), \tag{7.24b}$$

which correspond to the symmetric and asymmetric modes shown in Fig. 7.3. In addition, combining the dispersion relations in both regions yields the condition

$$(\kappa_{z1}d)^2 - (\kappa_{z2}d)^2 = (k_2^2 - k_1^2)d^2. \tag{7.25}$$

A mode that simultaneously satisfies Eqs. (7.24) and (7.25) is therefore a mode supported by the structure. An intuitive graphical representation of the solution can be obtained by looking at Fig. 7.5, where the equations have been represented as a set of curves depending on the ratio $(-\mu_1/\mu_2)$. The graphical representation of these modes, in Fig. 7.3, illustrates that one is symmetric whereas the other one is asymmetric, which refers to the profile of the electric field. By analogy to regular media where the electric field follows sine and cosine functions, the electric field in this case follows hyperbolic sine and cosine functions,* suggesting to term these modes "cosh" and "sinh," for the symmetric and asymmetric modes, respectively (Wu et al. 2003).

The existence and characteristics of a mode can be directly obtained from Fig. 7.5 once the configuration is determined, i.e. once the frequency of operation is known, the slab thickness d, as well as the material parameters (ε_1, μ_1) for the medium surrounding the slab and (ε_2, μ_2) for the slab. These parameters define a value for $(k_2^2 - k_1^2)d^2$ that maps onto a horizontal line in both panels. Note that an increase in frequency or in thickness simply corresponds to a translation of this line away from the $(k_2^2 - k_1^2)d^2 = 0$ line, in either direction depending on the material parameters. The intersection of the $(k_2^2 - k_1^2)d^2$ line with the guidance condition curves corresponding to the $(-\mu_1/\mu_2)$ ratio of interest yields the solution(s), if any, that are supported by the given configuration. It can then immediately be seen for example that when supported, the cosh modes do not have a cutoff frequency whereas the sinh modes do. As another example, the perfect lens situation (see Chapter 8)

*The demonstration is straightforward and is left as an exercise to the reader.

© 2009 by Taylor & Francis Group, LLC

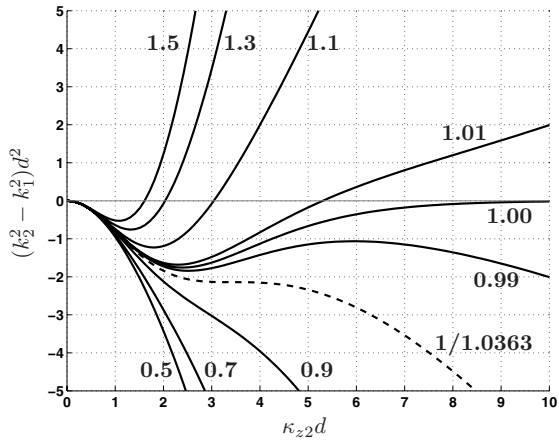

(a) Symmetric (cosh) modes.

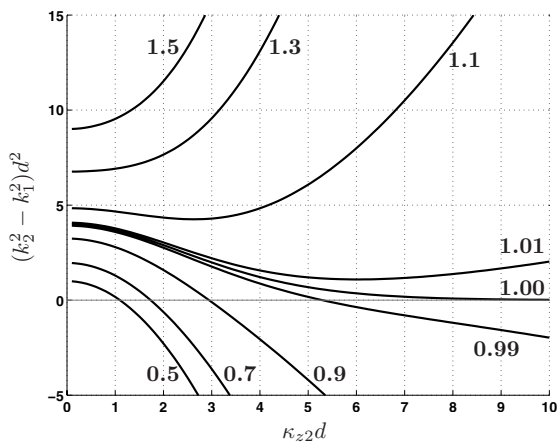

(b) Asymmetric (sinh) modes.

Figure 7.5 Graphical representation of Eqs. (7.24) and (7.25) as function of $\kappa_{2z}d$ for various values of $(-\mu_1/\mu_2)$ (indicated as numbers next to the curves).

corresponds to $k_2^2 - k_1^2 = 0$ and $-\mu_1/\mu_2 = 1.0$, for which it is seen that the intersecting point occurs at infinity.

The region $(k_2^2 - k_1^2)d^2 < 0$ can be accessed in two situations. The first corresponds to $k_2^2 < k_1^2$, i.e. a slab less dense than the background medium, supposing that all wavenumbers are real. The second situation, more unusual, occurs when the slab is made of a plasma medium, in which case k_2 is imaginary and $k_2^2 < 0$. The existence of hyperbolic modes in this case is well known (Oliner and Tamir 1962) and it is seen that these modes are identical

© 2009 by Taylor & Francis Group, LLC

to those supported by a slab of left-handed medium (for which k_2 is negative) when $|k_2| < |k_1|$. In particular, the specific value of $(-\mu_1/\mu_2 = 1/1.0363)$ was pointed out as being a limit above which a single mode propagation occurs and below which multi-modes are sustained. This conclusion is confirmed here graphically in Fig. 7.5(a).

The complex modes supported by the slab of left-handed media are therefore additional modes, which need to be accounted for. In particular, they coexist with the regular modes obtained when the transverse wavenumber in the slab is real. The guidance condition for these modes can be written as

$$\alpha_{z1} d = \frac{\mu_1}{\mu_2} (k_{z2} d) \tan (k_{z2} d/2) , \tag{7.26a}$$

$$\alpha_{z1} d = \frac{\mu_1}{\mu_2} (k_{z2} d) \cot (k_{z2} d/2) , \tag{7.26b}$$

$$(k_{2z} d)^2 + (\alpha_{z1} d)^2 = (k_2^2 - k_1^2) d^2 \tag{7.26c}$$

and is illustrated in Fig. 7.6. Since these modes have been extensively studied in the literature, for example in Collin (1990), we shall not study them in more detail here.

7.3 Negative refraction of surface plasmons

In analogy with the negative refraction of transverse electromagnetic waves at the interface between a positive index medium and a negative index medium, one can wonder whether it is possible to find interfaces between two surfaces where a surface plasmon wave refracts negatively. We show a schematic picture of such a process at the interface between the surfaces of two different media in Fig. 7.7. Since the surface modes are not purely transverse waves (there is a component of the fields along the wave-vector on the surface), we cannot examine if the waves are left-handed as for transverse waves in a three-dimensional negative refractive index medium. This question has been addressed by Kats et al. (2007) through an analysis of the relative directions of the energy flow based on the Poynting vector and the phase-vector $\mathbf{k}_{\|} = \hat{x} k_x + \hat{y} k_y$ on the surface.

For simplicity of calculations, we assume the zero dissipation limit where the imaginary parts of the material parameters are δ functions at the specified resonance frequencies, whereas at other frequencies, the media are assumed non-dissipative. Consider the dispersion for the P-polarized surface plasmon modes on a surface given by Eq. (7.4)

$$k_{\|} = \left[\frac{\varepsilon_1 \varepsilon_2 (\varepsilon_2 \mu_1 - \varepsilon_1 \mu_2)}{\varepsilon_2^2 - \varepsilon_1^2} \right]^{1/2} \frac{\omega}{c}.$$

© 2009 by Taylor & Francis Group, LLC

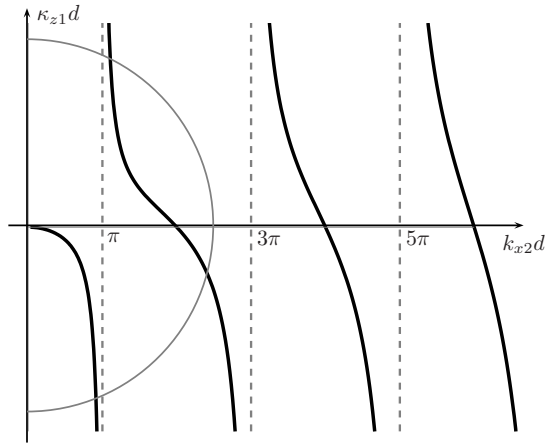

(a) Even modes.

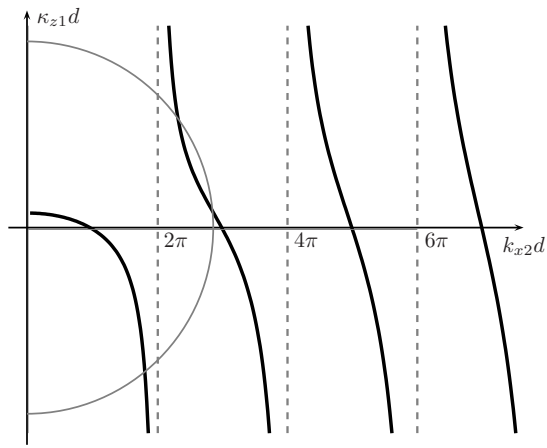

(b) Odd modes.

Figure 7.6 Illustration of the guidance condition in a regular waveguide configuration when the transverse wavenumber inside the slab is positive. In both cases, $-\mu_1/\mu_2 = 0.2$.

An essential condition for the existence of such modes is $\varepsilon_1\varepsilon_2 < 0$. The time averaged Poynting vector associated with such a mode given by $\mathbf{S} = (1/2)\mathrm{Re}(\mathbf{E}\times\mathbf{H}^*)$ is oppositely directed in the media on either side[†] and decays

[†]The demonstration is straightforward.

© 2009 by Taylor & Francis Group, LLC

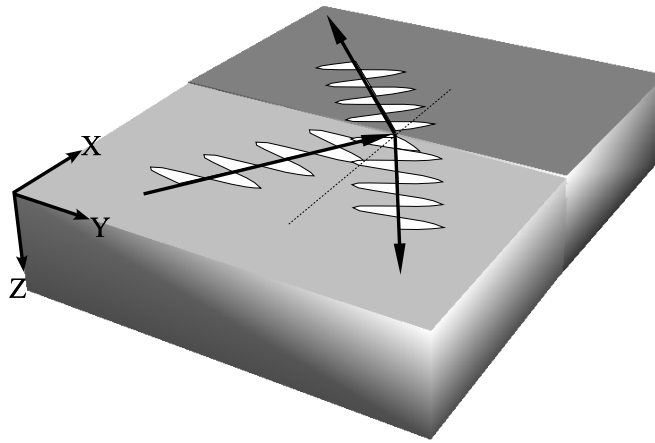

Figure 7.7 A schematic picture of surface plasmon modes at the surfaces of two media (shown by different shades of gray). The surface waves can undergo negative refraction at the interface between the two surfaces (media) as shown depending on the material parameters of the two media.

exponentially with distance from the interface

$$\mathbf{S} = \begin{cases} \frac{\mathbf{k}_\parallel}{\varepsilon_0 \varepsilon_1 \omega} |\mathbf{H}|^2 \exp(\kappa_{z1} z) & \forall\ z < 0, \\ \frac{\mathbf{k}_\parallel}{\varepsilon_0 \varepsilon_2 \omega} |\mathbf{H}|^2 \exp(-\kappa_{z2} z) & \forall\ z > 0. \end{cases} \tag{7.27}$$

One has to determine the energy flow along the interface associated with this surface mode. This can be accomplished by integrating the Poynting vector with respect to the normal z direction. We obtain for the integrated energy flow

$$\mathbf{W} = \int_{-\infty}^{\infty} \mathbf{S}\ dz = \frac{\mathbf{k}_\parallel}{\varepsilon_0 \omega \kappa_{z1} \varepsilon_1} \left[1 - \frac{\varepsilon_1^2}{\varepsilon_2^2}\right] |\mathbf{H}|^2. \tag{7.28}$$

Noting that $k_\parallel > 0$, $\varepsilon_1 > 0$, the condition for the wave-vector and the energy flow at the surface to be anti-parallel is

$$\varepsilon_1^2 > \varepsilon_2^2, \tag{7.29}$$

in which case such interfaces can be called *negative refractive interfaces*.

Note that the interface of an ordinary metal with $\varepsilon_2 < 0,\ \mu_2 = 1$, and vacuum cannot satisfy the above condition as no surface plasmon modes exist for $\varepsilon_1 > |\varepsilon_2|$. Consider, however, an interface between vacuum and a medium with $-1 < \varepsilon_2 < 0,\ \mu_2 < 0$: a surface plasmon mode on the interface with oppositely directed wave-vector and energy flow can be excited if $\varepsilon_2 - \mu_2 < 0$. This is the only kind of negative refractive interface possible for P-polarized

© 2009 by Taylor & Francis Group, LLC

modes when one of the media involved is vacuum. The conditions for the negative refractive interfaces with different media can be divided into six cases and the different ranges for $\varepsilon_1/\varepsilon_2$ and μ_1/μ_2 for which one has negative refractive interfaces are shown in Fig. 7.8.

The group velocity of the surface waves, $v_g = (\partial\omega)/(\partial k_\parallel)$, is negative on the negative refractive interfaces. This reflects the fact that the energy flow is opposite to the wave-vector on these interfaces. The dispersion curve for the P-polarized light when $\omega_{mp} > \omega_p$ shown in Fig. 7.2 clearly has a negative slope. For $k_\parallel \sim k_0$, the group velocity of the surface mode ($v_g = (\partial\omega)/(\partial k_\parallel)|_{\omega_0}$) can be expressed in terms of the wave group velocity in the two media. Consider the Taylor expansion for the dispersion equation $\varepsilon(\omega)\mu(\omega)\omega^2/c^2$:

$$\omega^2/c^2\varepsilon(\omega)\mu(\omega) = k_0^2 + 2k_0\frac{\partial k}{\partial\omega}|_{\omega_0}\delta\omega + \mathcal{O}(\delta\omega)^2, \tag{7.30}$$

where we retain only terms linear in the frequency difference, and the dispersion equation for the waves in the two media

$$\kappa_{z1}^2 = k_\parallel^2 - \varepsilon_1(\omega)\mu_1(\omega)\omega^2/c^2,$$
$$\kappa_{z2}^2 = k_\parallel^2 - \varepsilon_2(\omega)\mu_2(\omega)\omega^2/c^2.$$

For $k_\parallel \sim k_0$, substituting the expansion above into the right-hand side of the equation, we obtain

$$v_g = \frac{v_1 v_2(\kappa_{z1}^2 - \kappa_{z2}^2)}{v_1\kappa_{z1}^2 - v_2\kappa_{z1}^2}, \tag{7.31}$$

i.e. one can understand the group velocity of the surface mode at an interface as a weighted average of the group velocities of waves in the two media. The meaning of this becomes very clear in the case when one medium has a negative refractive index and the other has a positive refractive index. A particularly interesting case occurs when $\varepsilon_1 = \mu_1 = +1$ and $\varepsilon_2 = \mu_2 = -1$, which results in a zero group velocity for all surface modes. The surface modes are completely degenerate at the frequency $\omega = \omega_s = \omega_{ms}$. Note that the case $|\varepsilon_1/\varepsilon_2| = 1$ and $|\mu_1/\mu_2| = 1$ corresponds to this special point in the case of (c) and (f) in Fig. 7.8 where there is no net energy carried by the surface wave in any direction: as $\kappa_{z1} = \kappa_{z2}$ in the two media, the oppositely oriented Poynting vectors on either side of the media cause the net energy flow along the surface to become zero. A more detailed discussion of this effect is offered in Chapter 8. In other media that do not support propagating modes at all (for example, metals or purely negative magnetic permeability media), the meaning of this average for the group velocity becomes less clear and it is then more meaningful to talk of the energy associated with the surface mode rather than the group velocities within the individual media.

Consider Fig. 7.7 where we depict the interface (along the $y - z$ plane) between the two media with different properties which support surface states in the xy plane. If one surface supports modes with a positive wave-vector

© 2009 by Taylor & Francis Group, LLC

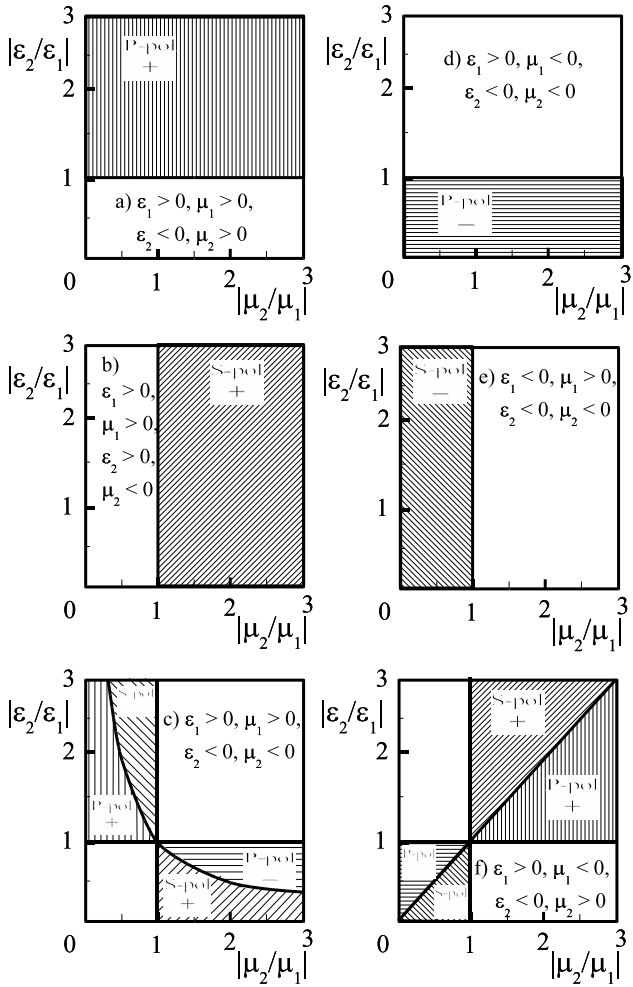

Figure 7.8 The six cases of negative refractive interfaces that are possible between media with different ε and μ. The parameter ranges when the interfaces support surface modes and have negative refractive interface (shown by a $-$ sign) or a positive refractive nature (shown by a $+$ sign) are marked by different gray shades for P-polarized and S-polarized surface modes. No surface modes are possible in the white regions. Redrawn based on the data of Kats et al. (2007).

© 2009 by Taylor & Francis Group, LLC

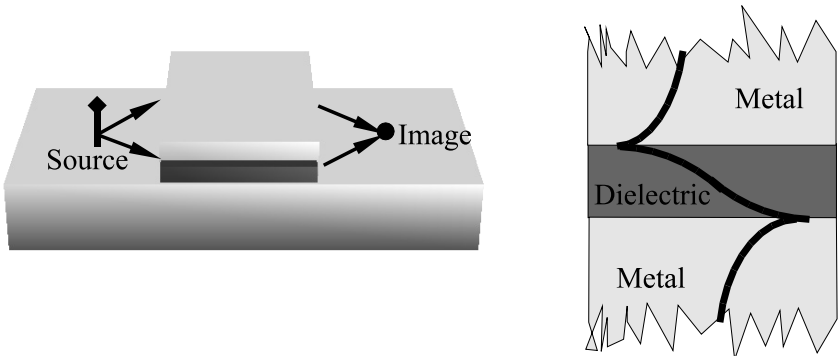

Figure 7.9 A schematic picture of the negative refraction of surface plasmon modes on a metal surface by coupling to the slab modes of a heterostructure. Negative refraction is enabled when the slab modes, particularly the anti-symmetric modes, have anti-parallel energy flow and wave-vector (shown on the right). The heterostructure acts as a flat lens focusing a point source placed on one side.

while the other surface supports modes with a negative wave-vector, it is clear that an incident surface wave is going to refract negatively across the interface between the two surfaces as depicted in the figure. This is in complete analogy with the negative refraction of transverse electromagnetic waves across the interface between two media: one positively refracting and one negative refracting. Note that there is a reflected wave from the interface as well. The solid arrows depict the energy flow. On one of the two surfaces the wave-vector on the surface has to be opposite to the energy flow. The reflection and transmission coefficients can also be calculated for these surface modes if one includes the fields of the resonant states at the interface between the two surfaces.

Another way to accomplish negative refraction of surface plasmon modes is to use a waveguide structure as shown in Shin and Fan (2006). The central idea is to couple the surface plasmon modes propagating on the surface into a waveguide-like structure where the guided modes have an energy flow opposite in direction to the wave-vector. This can be done as shown in Fig. 7.9 by using a metal-dielectric-metal structure where the metal is assumed to have a negative dielectric permittivity. It can be easily seen that the positive dielectric layer enclosed by the negative dielectric metal supports symmetric and anti-symmetric combinations of the surface plasmon modes as discussed earlier. Noting that the Poynting vector is oriented in opposite directions on either side of the metal-dielectric interface (due to change in the sign of the permittivity as discussed before), the flow of energy associated with the waveguide mode can be either parallel or antiparallel depending on whether the field is more concentrated in the dielectric or extended out to the metallic

© 2009 by Taylor & Francis Group, LLC

regions. The anti-symmetric mode is seen to extend out in the metallic regions under the appropriate conditions and can have a negative energy flow associated with it. Hence coupling the surface plasmon waves on the metal surface to the slab waveguide modes as shown in Fig. 7.9 results in negative refraction of the energy. The slab waveguide of finite width acts as a flat slab for surface plasmon waves. The exact conditions for an imaging geometry of a slab lens can be found in Shin and Fan (2006). Thus, not only surface modes, but slab modes can also be utilized for such purposes.

7.4 Plasmonic properties of structured metallic surfaces

In recent years, structured metallic surfaces and films have been shown to exhibit a wide variety of interesting plasmonic properties and novel phenomena [see Maier (2007) for a detailed exposition on this topic]. The prime among these effects is the extra-ordinary transmission of light through an array of subwavelength sized holes in a thick metallic film first described in Ebbesen et al. (1998). The problem of transmission of light through a small hole in a perfectly conducting surface is one of the few exactly solvable problems in rigorous diffraction theory (Bethe 1944) and predicts a transmitted intensity that is proportional to $(a/\lambda)^4$ (note that the similarity to the result from Rayleigh theory). In the experiments of Ebbesen et al. (1998), it was found that the transmittance through the array of subwavelength sized holes could be very high ($\sim$90% of the incident light at certain resonant frequencies). This intriguing result of high transmittance was later shown to hold even for single holes provided the region around the hole had been suitably patterned, for example, by having ridges of the metal in concentric circles (Barnes et al. 2003). The resonant tunneling through single subwavelength holes can be controlled by any embedded non-linear medium and has also been used to demonstrate a "photon blockade" effect (Smolyaninov et al. 2002) akin to the Coulomb blockade effect in mesoscopic quantum dots. The surface plasmon modes on the metal and the modes in the holes appear to play a crucial role in these phenomena.

In this section, we discuss a general issue related to structured metallic surfaces and films including structured perfectly conducting surfaces: i.e. their ability to support surface modes (Pendry et al. 2004). Note that a plain flat perfect conductor cannot support any surface modes, so that these plasmon modes were termed as "spoof" surface plasmon modes in Pendry et al. (2004). The structuring of the surface, however, appears to bring in an ability to support surface modes. It turns out that a distinction between these structure-induced surface modes and true surface plasmon modes on the structured surface of a metal with negative dielectric permittivity might not even be

© 2009 by Taylor & Francis Group, LLC

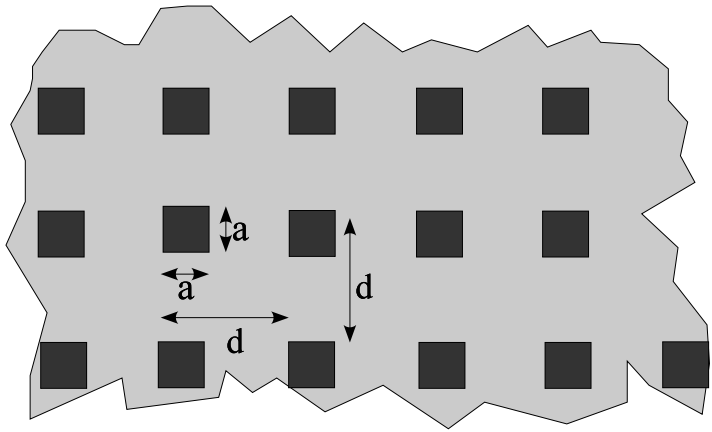

Figure 7.10 A film of a perfect conductor with an array of periodically placed square holes behaves as a plasma medium and can support surface plasmons.

possible as the excitations blend into each other. We discuss here only this general property as proposed in Pendry et al. (2004) while avoiding extended discussions of the large number of properties of subwavelength structured metallic films as well any controversies about their explanations in terms of the surface modes (Lezec and Thio 2004).

Consider a film of a perfectly conducting material containing periodically placed small holes (assumed square for simplicity) that go through the thickness of the film as shown in Fig. 7.10. Let the thickness of the film be t and the holes have a side of a placed on a square lattice of period d. Assume that the conditions for a homogeneous description of the surface are satisfied, i.e. $a < d \ll \lambda$ and consider radiation (with the electric field $\mathbf{E}$ along the y axis) to be incident on the film. The fields inside the perfectly conducting regions are zero and the fields exist only inside the holes. The incident radiation would primarily couple to the fundamental waveguide mode in the holes as higher modes decay faster with distance inside the hole. Consequently we can write the fields inside the holes as

$$\mathbf{E} = \hat{y} E_0 \sin(\pi x/a) \exp[\mathrm{i}(k_z z - \omega t)], \tag{7.32}$$

where $k_z = \sqrt{\varepsilon_i \mu_i \omega^2/c^2 - (\pi/a)^2}$ and the subscript i refers to the medium in the interior of the holes. We would like to replace the structured film by a film of some equivalent material where we have the averaged macroscopic field

$$\mathbf{E}_{\mathrm{av}} = \hat{y} E_0' \exp[\mathrm{i}(k_x x + k_z z - \omega t)]. \tag{7.33}$$

© 2009 by Taylor & Francis Group, LLC

Due to the symmetry in the xy plane, we have $\varepsilon_x = \varepsilon_y$ and $\mu_x = \mu_y$. For fields applied parallel to the axis of the holes (z direction), from the continuity of the E_z and H_z fields along the axis of the holes, we obtain that the material parameters should be the volume weighted average of the permittivities and permeabilities of the material in the hole and the perfect conductor. Hence we obtain

$$\varepsilon_z \to \infty, \qquad \mu_z \to \infty. \tag{7.34}$$

This implies that the dispersion in the homogenized film is

$$\frac{k_x^2}{\mu_z} + \frac{k_z^2}{\mu_x} = \varepsilon_y \frac{\omega^2}{c^2} \quad \Rightarrow \quad k_z = \pm\sqrt{\mu_x \varepsilon_y}\frac{\omega}{c}. \tag{7.35}$$

There is no dispersion of the modes with k_x or k_y for either polarization.

The average fields in the region of the film can be obtained as a volume average:

$$E_0' = \frac{E_0}{d^2}\int_0^a \mathrm{d}y \int_0^a \mathrm{d}x \ \sin(\pi x/a) = \frac{2a^2}{\pi d^2} E_0. \tag{7.36}$$

Another consistency condition would be that the component of the Poynting vector normal to the film has to be the same: whether calculated from the microscopic fields

$$(\mathbf{E}\times\mathbf{H})_z = \frac{-k_z E_0^2}{\mu_0\mu_i\omega}\frac{\int_0^a dy \int_0^a \sin^2(\pi x/a)}{d^2} = \frac{-k_z E_0^2}{\mu_0\mu_i\omega}\frac{a^2}{2d^2}, \tag{7.37}$$

or the macroscopic averaged fields

$$(\mathbf{E}_{\mathrm{av}}\times\mathbf{H}_{\mathrm{av}})_z = \frac{-k_z {E_0'}^2}{\mu_0\mu_x\omega}. \tag{7.38}$$

Although there are large inhomogeneous microscopic fields at the edges of the holes, we neglect these fields as they are localized (evanescent) and do not contribute to the energy flow. From the above two equations, we obtain

$$\mu_x = \frac{8a^2}{\pi d^2}\mu_i. \tag{7.39}$$

Noting now that k_z has to be the same in both cases, we obtain

$$\varepsilon_y = \frac{\pi^2 d^2}{8a^2}\left(1 - \frac{\pi^2 c^2}{\varepsilon_i\mu_i a^2\omega^2}\right), \tag{7.40}$$

which is similar to the dielectric function of a plasma with a plasma frequency $\omega_p = (\pi c)/(a\sqrt{\varepsilon_i\mu_i})$. This is actually the value for the lower cutoff frequency of the waveguide mode in the square hole configuration.

The structured metallic film is equivalent to a homogeneous plasma-like medium with the specified anisotropic material parameters. This film can essentially support slab plasmon polariton modes much like a plasma medium.

© 2009 by Taylor & Francis Group, LLC

In addition, the structure can enable weak coupling to propagating radiation. In general, the structures on the conducting film need not be holes, but could be bumps or any other structure that generates scattering modes that can be localized on the surface. However, the advantage of the hole-based geometry is to support a strong resonance, yielding a large response.

The homogenization view point is particularly useful for a dense set of small sized holes. Note that a discussion of the strong localized evanescent fields that would be present near the edges of the holes would be necessary for completeness of the description. These evanescent waves would be excited and would be required to account for the continuity of the fields at the surface of the conducting film. However, these evanescent modes do not contribute to the energy flow and can be neglected in the absence of dissipation in the film.

7.5 Surface waves at the interfaces of nonlinear media

We have seen in Section 3.6 that metamaterials can have nonlinear polarizability and magnetization. Thus, an interesting question concerns what happens to the surface modes at an interface if one or both media in question have nonlinear material parameters. This question assumes larger importance in view of the large local fields due to the surface states that enhance the nonlinear effects and drive the system into the nonlinear regime. Although nonlinear polarizabilities can be resonantly enhanced, it is advisable to remain reasonably away from the resonance as the unavoidable dissipation near the resonance itself effectively prevents both large local field enhancements and the expression of the nonlinear behavior. We essentially follow the approach of Shadrivov et al. (2004) here and present the elementary solutions for nonlinear surface modes on the interface of nonlinear metamaterials.

We specifically consider the case of third-order nonlinearities: $\chi_e^{(3)}$ and $\chi_m^{(3)}$ for both the electric polarization and the magnetization. For example, the SRR medium with Kerr nonlinear dielectric in the capacitive gaps has a Kerr-type nonlinear response at frequencies well away from the resonances where the system is bistable. In this case, the field at one frequency can act on itself through the nonlinearity (Boyd 2003) and the equation for the magnetic field of the P-polarized mode ($\mathbf{H}(x,z,\omega)$ is along $\hat{y}$ and $\mathbf{E}(x,z,\omega)$ lies in the xz plane) becomes a nonlinear Schrödinger equation:

$$\frac{\partial^2 H_y}{\partial x^2} + \frac{\partial^2 H_y}{\partial z^2} + \frac{\omega^2}{c^2}\left[\varepsilon(\omega)\mu(\omega) + \chi_m^{(3)}\varepsilon(\omega)|H_y|^2\right] H_y = 0. \tag{7.41}$$

Here the nonlinear polarization in the medium is taken to be

$$M_{NL} = \mu_0 \chi_m^{(3)} |H(x,z,\omega)|^2 H_y(x,z,\omega).$$

© 2009 by Taylor & Francis Group, LLC

There is a similar equation for the S-polarized mode, where the nonlinear electric polarization and the nonlinearity couple to the dispersion in μ. It is straightforward to see that an effective negative permittivity reverses the effect of self-focusing nonlinearity $\chi_m^{(3)} > 0$ to that of a non-focusing nonlinearity in a positive medium. Plane wave solutions in the nonlinear media can be written down by the ansatz:

$$H(x,z) = \xi(z)\exp[\mathrm{i}k_x x], \tag{7.42}$$

where for localized solutions we have

$$\xi(z) = A\ \mathrm{sech}[\kappa_z(z-z')], \tag{7.43}$$

and z' is a variable to be fixed by the boundary conditions. Implementing this into the nonlinear Schrödinger equation, we have that

$$\kappa_z^2 = k_x^2 - \varepsilon\mu\omega^2/c^2, \tag{7.44}$$

$$A = \kappa_z \left[\frac{2}{\chi_m^{(3)}\varepsilon}\right]^{1/2}. \tag{7.45}$$

Thus, we can have solitonic solutions for the surface modes and z' turns out to be the center of the soliton.

We can have interfaces between two nonlinear media or between one linear medium and a nonlinear medium. These have been dealt with comprehensively in Shadrivov et al. (2004). The solutions in different cases are pictorially shown in Fig. 7.11. Note that nonlinearity can induce surface modes even in cases where there exist no surface modes in the linear limit: for example, S-polarized surface modes on the interface between a negative dielectric and positive dielectric medium. Here we only consider the interface between vacuum ($\varepsilon = 1,\ \mu = 1$) for $z < 0$, and a medium with $\varepsilon_2 < 0$ and $\mu_2 < 0$ and nonlinear Kerr-type polarization ($\chi_e^{(3)}$) and magnetization ($\chi_m^{(3)}$) for $z > 0$. Then we have the magnetic fields of the P-polarized modes as:

$$H_y(x,z) = \begin{cases} H_0\ \exp[\mathrm{i}k_x x]\ \exp[\kappa_{z1} z] & \forall\ \ z < 0, \\ \kappa_{z2}\left[\frac{2}{\chi_m^{(3)}\varepsilon_2}\right]^{1/2} \exp[\mathrm{i}k_x x]\ \mathrm{sech}[\kappa_{z2}(z-z')] & \forall\ \ z > 0. \end{cases} \tag{7.46}$$

Enforcing the conditions on continuity of the tangential components of the fields at the interface, we get the conditions

$$H_0 = \kappa_{z2}\left[\frac{2}{\chi_m^{(3)}\varepsilon_2}\right]^{1/2} \mathrm{sech}[\kappa_{z2}(z')], \tag{7.47a}$$

$$-\frac{\kappa_{z1}\varepsilon_2}{\kappa_{z2}} = \tanh[\kappa_{z2} z'], \tag{7.47b}$$

© 2009 by Taylor & Francis Group, LLC

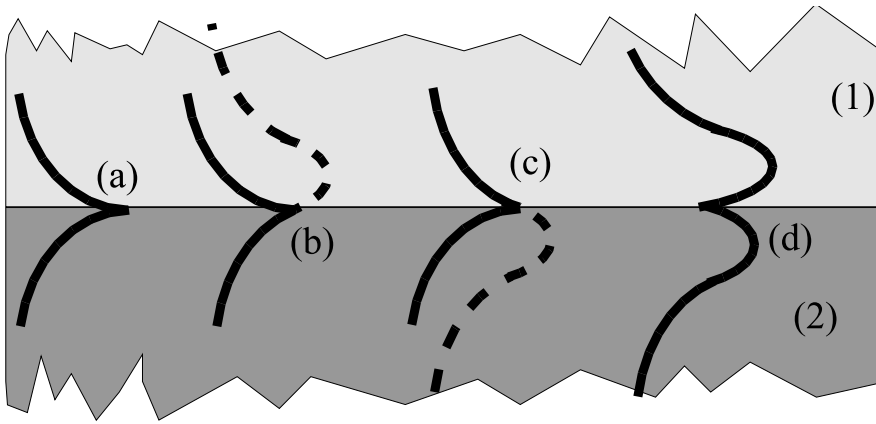

Figure 7.11 An interface between two media (1) and (2) can support a variety of surface waves, which are shown schematically: (a) Both media are linear. (b) Medium (1) is linear while medium (2) is nonlinear. (c) Medium (2) is linear while medium (1) is nonlinear. (d) Both media are nonlinear. The dashed line corresponds to the continuation of the sech solution into the other medium and peaks at the location of the displaced center of the solitonic solution (z').

from which we obtain the equation of dispersion for the nonlinear surface modes

$$\kappa_{z1} + \frac{\kappa_{z2}}{\varepsilon_2}\left(1 - \frac{\chi_m^{(3)}\varepsilon_2 H_0^2}{\kappa_{z2}^2}\right)^{1/2} = 0. \tag{7.48}$$

A similar equation can be obtained for the S-polarized modes as

$$\kappa_{z1} + \frac{\kappa_{z2}}{\mu_2}\left(1 - \frac{\chi_e^{(3)}\mu_2 E_0^2}{\kappa_{z2}^2}\right)^{1/2} = 0. \tag{7.49}$$

Note that the nonlinear contribution to the dispersion is essentially the nonlinear change of the dielectric permittivity or the magnetic permeability arising due to the particular field strengths. Further, the effect of the nonlinearity is more effective for smaller wave-vectors κ_{z2}. Typical numbers for these changes can be obtained by noting that some of the largest nonlinear coefficients for non-resonant Kerr processes in conventional nonlinear media are $\chi_e^{(3)} \sim 10^{-18}$ SI units. Hence even with surface electric fields of $E \sim 10^5$ V/m which occur in structured metallic surfaces with large local field enhancements, these corrections are of the order of 10^{-8}. However, for resonant processes or photorefractive processes, the nonlinear coefficients can be as large as $\chi_e^{(3)} \sim 10^{-12}$ SI units. In these cases, the corrections become of the order of 10^{-2} to 10^{-1}

© 2009 by Taylor & Francis Group, LLC

and nonlinearity can have large effects, particularly for small wave-vectors, and can even actually switch the dispersion of the surface modes from a negative group velocity to a positive group velocity as detailed in Shadrivov et al. (2004) if the non-linear terms are large enough. However, the large nonlinearities come at the cost of large time response implying that the large changes in the surface mode dispersions obtained with such enhanced nonlinear processes are probably of scant importance for plasmonic applications where fast switching speeds are required. However, they may well be important for many other applications.

© 2009 by Taylor & Francis Group, LLC